Sensors and Actuators A 261 (2017) 94–102

Contents lists available at ScienceDirect

Sensors and Actuators A: Physical

journal homepage: www.elsevier.com/locate/sna

Fluorine-chlorine co-doped TiO_2/CSA doped polyaniline based high performance inorganic/organic hybrid heterostructure for UV photodetection applications

Shivani Sharma, Robin Khosla, Dinesh Deva, Hitesh Shrimali, Satinder K. Sharma*

School of Computing and Electrical Engineering, Indian Institute of Technology (IIT)-Mandi, Mandi, Himachal Pradesh 175005, India

ARTICLE INFO

Article history:
Received 28 October 2016
Received in revised form 21 April 2017
Accepted 24 April 2017
Available online 29 April 2017

Keywords:
Organic/Inorganic
F-Cl-TiO_2
CSA-Polyaniline
Heterostructure
UV photodetector

ABSTRACT

Fluorine-Chlorine, co-doped TiO_2 and CSA, doped Polyaniline based n-p heterostructures (F-Cl-TiO_2/CSA-PANI) are fabricated on ITO-coated glass substrate by spin coating at room temperature. The Al/CSA-PANI/F-Cl-TiO_2/ITO, structures are highly sensitive to UV illumination with a considerable photo-to-dark current contrast ratio of ~381 at −1 V, exceptional ideality factor ~1.9, substantial barrier height ~0.73 eV at zero bias, significantly large responsivity ~24.9 A/W, photoconductive gain ~84.59 and reasonable rise/fall time ~0.6/1.6 s. The CSA-PANI/F-Cl-TiO_2 interface/surface morphology, phase analysis, elemental composition and the optical properties of F-Cl-TiO_2 are investigated by FESEM, X-ray diffraction, EDX and UV–vis spectroscopy. The significant enhancement in photo current is elucidated with the proposed energy band model and a corresponding collateral conduction mechanism as anticipated for the F and Cl doping in TiO_2 based hybrid photodiode. The long-living radiant trapping sites and enhanced photoactivity by F and Cl co-doping divulge a potential candidature of the heterostructure as an alternate for next generation UV photodetection applications.

1. Introduction

Ultraviolet (UV) photodetectors have drawn immense attention due to their demand in various applications ranging from industry, military, radiation detection, flame detection, optical communications, astronomical studies, chemical, medicine, environment and biological fields [1–4]. The state-of-the-art Si-based UV photodetectors have limitations due to the small Si band gap of 1.1 eV, which require expensive optical filters to terminate photons with low energy. Recently, research progress [5–9] of wide bandgap semiconductors such as SiC, GaN, TiO_2 and ZnO, etc. have eliminated the use of filters and opened pathways for next-generation high-performance and low cost UV photodetectors.

Among the above, TiO_2 has emerged as a prospective wide band gap semiconductor material for high performance UV photodetectors due to its large UV absorption coefficient, transparent in the visible region, superior electrochemical activity, high refractive index, low cost and non-toxicity [10]. It can be formed in three different polymorphs: the anatase (~3.2 eV), the rutile (~3 eV) and the brookite crystal structures [11]. The uniformity and quality of TiO_2 thin films depend on the deposition technique and the choice of substrate. There are several well-established physical and chemical techniques listed in literature [13–18] to deposit TiO_2 thin films such as, RF sputtering [13], pulsed laser deposition (PLD) [14], electron-beam evaporation [12], chemical bath deposition (CBD) [16], metal organic chemical vapour deposition (MOCVD) [15], spray pyrolysis [17] and sol-gel [18] etc. on various substrates such as, glass [11], quartz [12], Silicon [13], Fluorine-doped tin oxide (FTO)-coated glass [19], Indium-doped tin oxide (ITO)-coated glass [20]. Compared to the aforesaid deposition techniques, spin coating is an attractive process to deposit TiO_2 thin films due to its numerous advantages such as low-temperature deposition, easily controllable process parameters, ease of deposition, homogeneity on various substrates and requirement of low-cost production facilities [17,21].

In addition, conducting polymers are of great importance for optoelectronic devices due to their diversity in the structure, electrochemical and electrical properties, high processability from the solution, viz the simple and low fabrication cost [22–25]. From the conducting polymer family, CSA-doped Polyaniline (CSA-PANI) is a potential p-type semiconducting material with high chemical sta-

* Corresponding author.
E-mail addresses: hitesh@iitmandi.ac.in (H. Shrimali), satinder@iitmandi.ac.in (S.K. Sharma).

http://dx.doi.org/10.1016/j.sna.2017.04.043
0924-4247/

bility, high electrical conductivity, high environmental stability and low processing cost. Hence, CSA-PANI is extensively adopted in optoelectronic and electronic applications such as electrochromic displays rechargeable batteries, electronic switches, gas sensors, and photovoltaic devices [26,27]. Moreover, it is well reported that CSA-PANI synthesized using m-cresol as solvent exhibits superior electrical conductivity due to the formation of expanded coil formation [28,29].

In the past decade literature, numerous studies have been conceded to tailor the band gap of TiO_2 by doping with metals (Ce [30], Cr [31], Fe [32], La [33], Ru [22], V [23]) and non-metals (B [24], C [25], F [34], N [35], P [36], S [37]) to augment the optical properties of TiO_2 in the visible and UV regions. Amid the aforesaid, metal ion doping of TiO_2 reduces its thermal stability and introduce recombination centers especially at increased doping levels, whereas non-metal ion doping of TiO_2 has become a favored research topic [38]. Among the non-metals, halogen ions (F [32], I [39], Cl [40], Br [41]) have attracted enormous attention as a dopant for TiO_2 because of their capability to narrow the band gap and improve the UV activity [40]. In addition to single ion doped TiO_2, co-doped TiO_2 offers better utilization of sunlight in the visible range and enhanced detection in UV range [38]. Thus, co-doped TiO_2 has attracted the immense attention of scientific community particularly for photodetection applications.

Likewise, in recent years, a number of TiO_2 based photodiode structures such as Schottky [42,43], metal-semiconductor-metal (MSM) [44], *n*-TiO_2/p-TiO_2 homojunction [45] and TiO_2 thin film based heterojunction devices [10,11,46] have been explored for UV detection. Among the above structures, the *n*-TiO_2/p-PANI hybrid heterostructure is attractive due to its low-temperature processing, flexible nature and highly advanced electronic, electrical, sensing and heterojunction properties [47,48].

In respect of the above, Liu et al. reported TiO_2/PANI heterostructure for solar cell applications [47] and Ameen et al. reported the diode behaviour of PANI/TiO_2 heterostructure [48,49]. In addition, Dozzi et al. observed that doping TiO_2 with Fluorine (F) induces surface, bulk defects and long-living radiant surface trapping sites (tens of nanoseconds or more) that are beneficial for photoactivity [50] and Xu et al. fabricated a high performance Chlorine (Cl)-doped TiO_2 using soft interface method for solar cell device applications [51]. However, limited literature is found regarding the doped TiO_2/PANI, n-p heterostructure especially for UV detection applications. The idea is to use the long-living radiant surface trapping sites by Fluorine doping and enhanced photoactivity obtained by Chlorine doping.

In this work, first time spin coated F-Cl-TiO_2/CSA-PANI, n-p heterostructure is fabricated on ITO coated glass. The electrical characteristics i.e. Current-Voltage (I–V), Current-Time (I-T) measurements are obtained in the dark and under the UV illumination with a 365 nm light (intensity ~35 $\mu W/cm^2$). Moreover, the thermal stability and the effect of lateral/vertical conduction in Al/F-Cl-TiO_2/CSA-PANI/ITO, structure is investigated by I–V measurements with variation in temperature and electrode area, respectively. F-Cl-TiO_2/CSA-PANI interface analysis is investigated by cross-sectional Field Emission Scanning Electronic Microscopy (FESEM). Furthermore, to support the significant enhancement in photo-conduction the F-Cl-TiO_2 powder which is used for thin film deposition is examined for the surface morphology, crystallinity, chemical composition and the optical properties by FESEM, X-ray diffraction (XRD), Energy dispersive X-Ray Analysis (EDX), and UV–vis spectroscopy, respectively. Finally, the noteworthy improvement in photo current of Al/F-Cl-TiO_2/CSA-PANI/ITO hybrid system is elucidated with the suitable energy band diagram and an anticipated conduction mechanism for F and Cl doping in TiO_2 based hybrid photodiode system.

2. Experiment

2.1. Materials

The titanium (IV) isopropoxide (TIP) was procured from Sigma Aldrich (purity 97%). The monomer aniline (purity 99%), oxidant Ammonium peroxydisulphate (APS) (purity 98%), hydrochloric acid (HCl), sodium chloride (NaCl), Isopropyl alcohol (IPA) and hydrofluoric acid (HF) are provided by Fisher Scientific. The doping material camphor sulfonic acid (CSA) was purchased from Alfa Aesar. The solvents ethanol and m-cresol (purity 99.5%) were acquired from Merck and TCI Chemicals, respectively. Note that, all the chemicals were utilized as received without any additional purification. The Deionized (DI) water (resistivity ~18.2 MΩ/cm) obtained by ELGA water purification system was used during the cleaning and solution preparation processes.

2.2. Synthesis of polyaniline

Polyaniline is synthesized chemically at ~0–5 °C by the oxidation process. Initially, 0.22 M aniline monomer is dissolved in 100 ml of 1 M HCl and the solution chilled at ~0 °C (Fig. 1(i)). Then, 33 ml of 0.8 M solution of ammonium peroxydisulphate ($(NH_4)_2S_2O_8$) in HCl (1 M) solution (Fig. 1(ii)) was added to monomer aniline solution dropwise for 2 h with continuous stirring at ~0–5 °C (Fig. 1(iii)) and thereafter stirring further continued for 4 h at ~0–5 °C(Fig. 1(iv)). Next, the solution was kept for 12 h at 0 °C to allow settling down of the resultant polymerized PANI precipitates, followed by acetone and then DI water rinse to remove the aniline oligomers (Fig. 1(v)). Further, the precipitates were vacuum dried for 12 h at 60 °C to obtain emeraldine PANI powder (Fig. 1(vi)). Ensuing to this, the CSA powder is added to Polyaniline powder (Fig. 1(vii)) followed by addition of m-cresol solvent (Fig. 1(viii)) in the ratio of PANI (1): CSA (5): m-cresol (20). Finally, the solution is stirred at 90 °C for 1 h followed by ultrasonic treatment for 12 h to obtain a homogeneous CSA-PANI solution (Fig. 1(ix)).

2.3. Synthesis of F-Cl Co-doped titanium dioxide powder

The sol-gel synthesis technique is used for TiO_2 and F-Cl doped TiO_2 preparation. Here, TIP, HF and NaCl are used as the TiO_2 precursor, Fluorine dopant and Chlorine dopant, respectively. Whilst, pure TiO_2 is prepared in the absence of dopants. Initially, 8.5 ml of IPA was added to 20 ml of a mixed aqueous solution of NaCl and HF under vigorous stirring at 27 °C (Fig. 1(x)). After 5 min, 0.6 ml of TIP was dropwise added to this solution with continued stirring for 4–6 h at 27 °C until a whitish slurry solution of dispersed TiO_2 is obtained (Fig. 1(xi)). Next, the alcohol and water are evaporated from the solution at 60 °C for 12 h in air to obtain F^- and Cl^- doped TiO_2 powder (Fig. 1(xii)). Finally, the obtained F-Cl-TiO_2 powder was calcined at 200 °C in a vacuum oven to form amorphous TiO_2 (Fig. 1(xiii)).

2.4. Fabrication of n-p heterostructure

Initially, the ITO coated glass is cleaned with soapy water for 15 min, followed by ultrasonication, sequentially in DI Water, Acetone, Ethanol, and DI water for 15 min each. The synthesized formulation of TiO_2 was spin coated on cleaned ITO coated glass at 3000 rpm for 30 s with 18 coating cycles to obtain the thin film of TiO_2. Ensuing this, the deposited TiO_2 thin films are annealed for 20 min at 100 °C to evaporate the ethanol solvent. Further, the CSA-PANI solution was spin coated over TiO_2 thin films at 4000 rpm for 90 s with 28 coating cycles to form the CSA-PANI/F-Cl-TiO_2 heterostructure followed by annealing at 60 °C for 10 min to evaporate the m-cresol solvent. Finally, for the top ohmic contact,

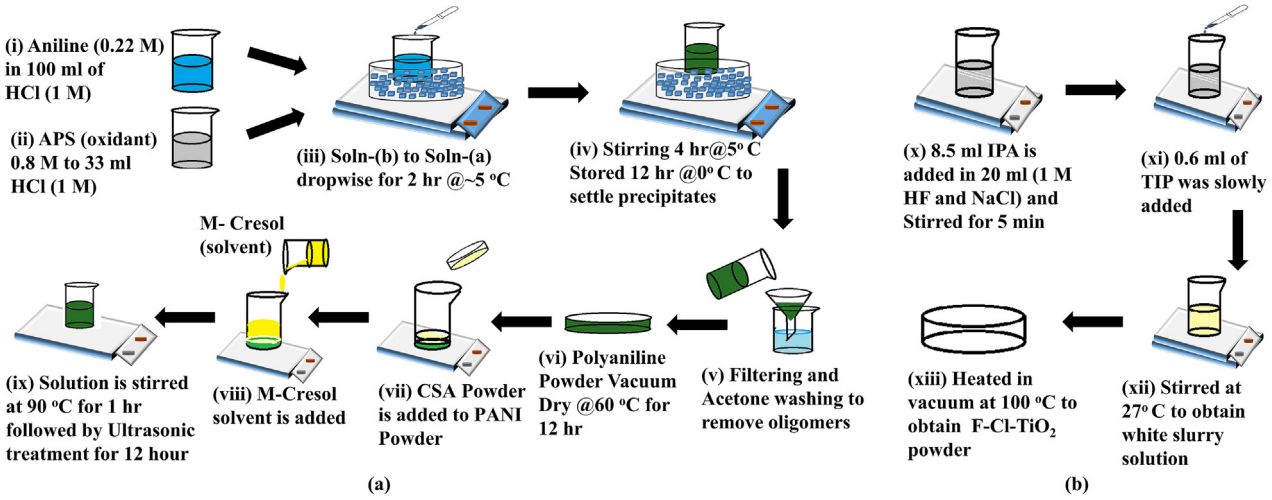

Fig. 1. Synthesis of CSA-PANI using Chemical Oxidation method by polymerization of aniline (i)-(ix), (b) Synthesis of F-Cl-TiO_2 using Sol-Gel Method (x)-(xiii).

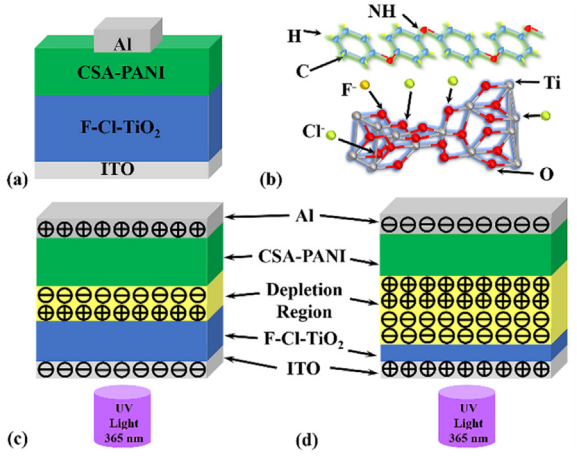

Fig. 2. The Al/CSA-PANI/F-Cl-TiO_2/ITO, organic/inorganic heterostructure device, (a) structure, (b) PANI/TiO_2 crystal structure (C-Blue, H-Yellow, NH-Red in PANI and Ti-Grey, O-Red, F-Yellow, Cl-Green in TiO_2) (c) under forward bias condition, and (d) under reverse bias condition. (For interpretation of the references to colour in this figure legend, the reader is referred to the web version of this article.)

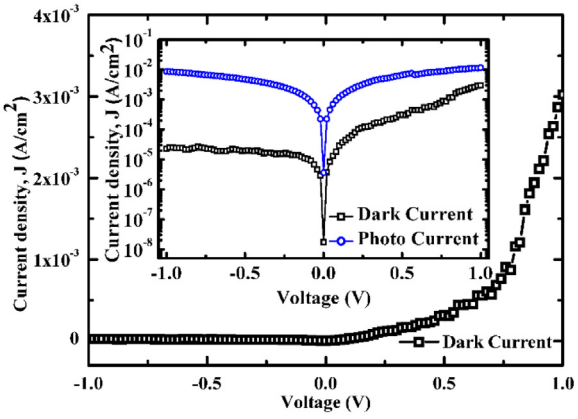

Fig. 3. Current density-Voltage (J-V) Characteristics of Al/CSA-PANI/F-Cl-TiO_2/ITO, structure. The inset shows the semi-log plot of dark and photo (365 nm illumination) J-V characteristics of Al/CSA-PANI/F-Cl-TiO_2/ITO, structure.

rectangular Aluminium electrodes of area 0.1 cm^2 are thermally evaporated at an ultimate pressure of 3×10^{-6} torr, to obtain the Al/CSA-PANI/F-Cl-TiO_2/ITO, structure as shown in Fig. 2(a). Here the crystal structure of CSA-PANI/F-Cl-TiO_2 is shown in Fig. 2(b) [70,71], where it is represented that few F^- atoms replace the O atoms in TiO_2 whereas the majority of Cl^- atoms replace O atoms and few Ti atoms also. Furthermore, Al/CSA-PANI/F-Cl-TiO_2/ITO, structure under the forward bias at 1 V and reverse bias at −1 V, is shown in Fig. 2(c), 2(d), which shows the width of depletion region increases under reverse bias.

2.5. Characterizations

The thicknesses of deposited F-Cl-TiO_2 (~270 nm), CSA-PANI (~100 nm) and Aluminium (~100 nm) thin films are estimated by Nanomap-LS Profilometer and also further confirmed by cross-sectional Field Emission Scanning Electron Microscope (SEM). The electrical characteristics are determined using Keithley SCS 4200 system in dark and under 365 nm UV illumination from UV lamp (power 35 μW/cm^2). The surface morphology and elemental composition are investigated by Field Emission Scanning Electron Microscope (FESEM) (JFEI, USA) and Electron Dispersive X-rays diffraction (EDX), respectively. The chemical phases are investigated by the X-ray diffraction (XRD) of Agilent Supernova diffractometer, Co Kα source (λ = 1.5418 A°) at an accelerating current and voltage of 0.80 mA and 50 kV, respectively. The UV–vis spectroscopy is performed for 200–800 nm wavelength using the UV-2450 from Shimadzu.

3. Results and discussions

The current density-voltage (J-V) characteristics of Al/CSA-PANI/F-Cl-TiO_2/ITO, structure obtained by sweeping the voltage from −1 to +1 V are shown in Fig. 3. The Al/CSA-PANI/F-Cl-TiO_2/ITO, structure shows a rectifying behavior with a rectifying ratio (i.e. the ratio of forward (I_f) to the reverse (I_r) current) of ~132 at a bias voltage of |1V|, attributes to the formation of heterojunction diode between CSA-PANI/F-Cl-TiO_2. From Fig. 3, it is clearly observed that F-Cl-TiO_2/CSA-PANI, n-p heterostructure operates in two regions, i.e. low injection region from 0.0 to 0.5 V and high injection region from 0.5 to 1.0 V. As perceived from Fig. 3, at lower voltage (0.0–0.5 V), the F-Cl-TiO_2/CSA-PANI, n-p heterostructure operates in low injection region due to electron-hole pair generation-recombination in the depletion region and results in the slight variation of the heterostructure current. When the applied voltage varies from 0.5 to 1.0 V, the F-Cl-TiO_2/CSA-PANI structure operates in high injection region and results in the rapid increase

of heterostructure photo current. While in the reverse bias region from −1 to 0 V, depletion width becomes wider and the minority carriers diffuse across the depletion region that are swept by the applied field and contribute significantly to the reverse current [52].

The semilog J-V characteristics of Al/CSA-PANI/F-Cl-TiO_2/ITO, structures are shown in the inset of Fig. 3, obtained by the voltage sweep from −1 to +1 V under dark and under 365 nm UV illumination. From the inset of Fig. 3, it is evident that there is a significant variation in both the forward and reverse current on UV illumination, ascribed to the generation of electron-hole pairs by the process of photogeneration. However, the variation of reverse current is higher because in reverse bias the width of the depletion region of F-Cl-TiO_2/CSA-PANI, structure is large that reveals the generation of a higher number of electron-hole pairs, as compared to that in the forward bias of n-p heterostructure.

Hence, the Al/CSA-PANI/F-Cl-TiO_2/ITO, structure depicts photodetector properties, with the contrast ratio (i.e. the ratio of the photocurrent (I_{ph}) to the dark current (I_d)) of ~381 at −1 V. Therefore, the significantly higher rectifying ratio ~132 and contrast ratio ~381 of the n-p heterostructure, supports its potential candidature as an efficient UV photodetector. The measured I–V characteristics of the Al/CSA-PANI/F-Cl-TiO_2/ITO, structure is substantiated by the standard thermionic emission theory, as follows [53,54]:

$$I = I_o\left[exp\left(\frac{q}{\eta kT} - 1\right)\right] \quad (1)$$

$$I_o = AA^*\left[exp\left(-q\frac{\phi_{Beff}}{kT}\right)\right] \quad (2)$$

where, q, η, A, A^*, T, I_o, K, and ϕ_{Beff} are the electronic charge, the ideality factor of the heterojunction, contact area, Richardson constant (≈1200 $Acm^{-2}K^{-2}$ for TiO_2) [54,56], temperature, the reverse saturation current, the Boltzmann constant, and the barrier height, respectively. Here, the reverse saturation current (I_o) of ~6.36×10^{-6} A is measured by the extrapolation of the linear region in the dark ln (I)-V characteristics from the inset of Fig. 3 [55]. This extremely low reverse saturation current reveals high-quality F-Cl-TiO_2/CSA-PANI structure. Moreover, the value of $I_o \sim 6.36 \times 10^{-6}$ A is smaller than the reported *n*-TiO_2/p-Si (~12 μA) [55] and *n*-Al-B-ZnO/p-Si, (~1.6–2.6 mA) [59]. Using Eqs. (1) and (2), the effective barrier height at zero bias (ϕ_{Beff}) and the ideality factor (η) are calculated from the following relations for Al/CSA-PANI/F-Cl-TiO_2/ITO, heterostructures [55–59]:

$$\phi_{Beff} = \frac{kT}{q} ln\left(\frac{AA^*T^2}{I_o}\right) \quad (3)$$

$$\eta = \left(\frac{q}{kT}\right)\left(\frac{\partial V}{\partial \ln(I)}\right) \quad (4)$$

Using Eqs. (3) and (4), the ϕ_{Beff} and η for F-Cl-TiO_2/CSA-PANI, systems are estimated ~0.728 eV and ~1.9, respectively. The exceptional ideality factor of ~1.9 for F-Cl-TiO_2/CSA-PANI, n-p heterostructure, computed here is better than the NC-ZnO (7.95) [9], *n*-TiO_2/p-Si (~3.83) [55], *n*-ZnO/p-Si (~2.3–4.21) [60,61], *n*-ZnO/p-GaN (~7–24) [62] and comparable to *n*-Al-B-ZnO/p-Si (~1.6–2.4) [59]. Nevertheless, *n*-Al-B-ZnO/p-Si suffered from high reverse saturation current ~1.6 mA, which limits its application for commercial scale high sensitivity UV detector applications. The F-Cl-TiO_2/CSA-PANI, system consists ~252 times less reverse saturation current than reported elsewhere [59], which reveals high-quality of fabricated n-p heterostructure due to significantly lower reverse leakage current. The responsivity (R_{UV}), and the photoconductive gain (g) of F-Cl-TiO_2/CSA-PANI structure is computed from the following relation [55,57,58]:

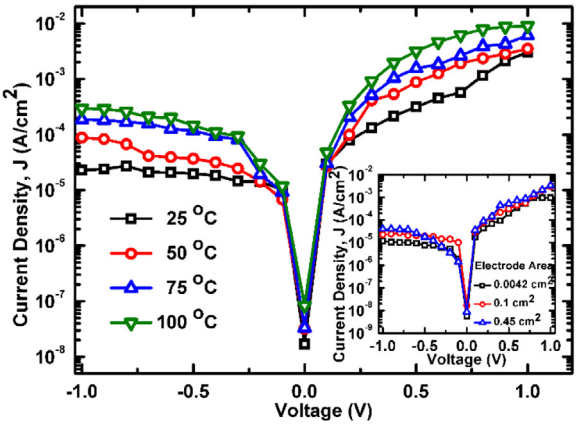

Fig. 4. Current density-Voltage (J-V) Characteristics of Al/CSA-PANI/F-Cl-TiO_2/ITO, structure with variation in temperature of 25, 50, 75 and 100 °C. The inset shows the J-V plots of Al/CSA-PANI/F-Cl-TiO_2/ITO, structure with variation in Al electrode area.

$$R_{UV} = \frac{I_{PH}}{P_{opt}} \quad (5)$$

$$g = \frac{1240 \times R_{UV}}{\lambda\,(nm) \times EQE} \quad (6)$$

where, I_{PH}, P_{opt}, λ (nm), and EQE, are the photocurrent at −1 V, the optical power, the wavelength (in nm) of the incident UV light, and the external quantum efficiency (EQE assumed 1 for calculations [55]), respectively. Using Eqs. (5) and (6), the responsivity (R_{UV}) and photoconductive gain (g) of F-Cl-TiO_2/CSA-PANI structure is calculated ~24.9 A/W and 84.59, respectively, which are much higher than the existing photo detector literature [55,59–62,71].

Moreover, for real world photodetector applications the photo diode must have good thermal stability and reliability. Thus, the thermal stability analysis of F-Cl-TiO_2/CSA-PANI (n-p) photodiodes is performed from 25 to 100 °C. Fig. 4 shows the current density-voltage (J-V) characteristics of Al/CSA-PANI/F-Cl-TiO_2/ITO, structure with variation in temperature of 25, 50, 75 and 100 °C. As revealed from Fig. 4, the current density of the Al/CSA-PANI/F-Cl-TiO_2/ITO photodiode increases with increase in temperature. As it is well established that TiO_2 will only show any significant variation in conductivity due to phase change at higher tempertaure (> 400 °C), whereas the maximum temperature applied, here in this thermal study is well below. It clearly indicates that this significant enhancement in the hybrid photo diode current with increase in temperature is because of higher charge transfer between CSA and PANI and also might be due to PANI molecular rearrangment or motion at such a high temperature treatment. Which results the more ordered polyaniline chain due to molecular level motion or rearrangment of dopant in the polymer chain that leads to enhanced conductivity, similar observations are also reported elsewhere in the literature [72]. Although, the increase in current density with variation of temperature is in bearable range, which attributes to a good thermal stability of the fabricated Al/CSA-PANI/F-Cl-TiO_2/ITO, structure and its potential condidature for real world photodiode applications.

Further, to verify that the observed electrical response of the Al/CSA-PANI/F-Cl-TiO_2/ITO, structure is due to vertical charge transport and not due to the lateral contribution, another set of Al/CSA-PANI/F-Cl-TiO_2/ITO, samples were fabricated with similar fabrication steps and also from same batch but of different electrode area and the corresponding measured, J-V characteristics are shown in the inset of Fig. 4. The calculated current density

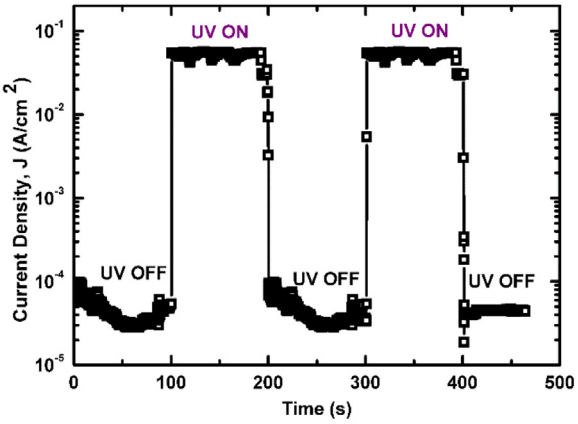

Fig. 5. Current density-Time (J-T) Characteristics of Al/CSA-PANI/F-Cl-TiO_2/ITO, structure at −1 V bias, where the UV light is illuminated after alternate 100 s.

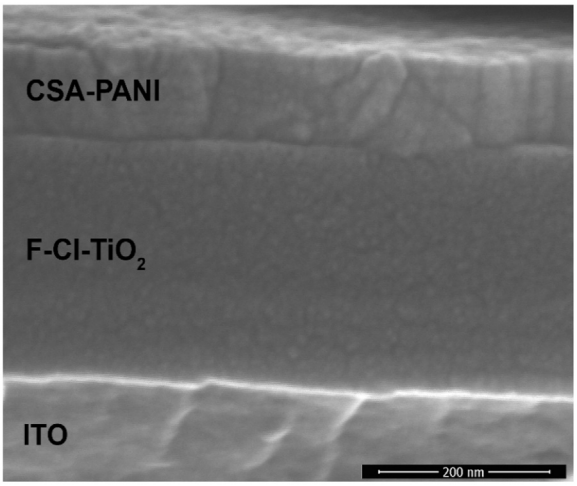

Fig. 6. Cross-sectional FE-SEM image of the F-Cl-TiO_2/CSA-PANI, n-p heterostructure.

for Al/CSA-PANI/F-Cl-TiO_2/ITO, structure is ~1.9×10^{-5}, 2.2×10^{-5} and 4.0×10^{-5} A/cm^2 at −1 V gate voltage with electrode areas of 0.0042 cm^2, 0.1 cm^2 and 0.45 cm^2, respectively. This negligible variation in current density, ~1% with respect to the large variation in electrode area ~100% attributes that the conduction path in Al/CSA-PANI/F-Cl-TiO_2/ITO, photodiodes is due to the vertical charge transport underneath the Al top electrode i.e. starting from Al electrode and reaching the ITO electrode through CSA-PANI/F-Cl-TiO_2 layer. Moreover, the small shunt resistance in vertical direction due to much smaller thickness of the PANI and TiO_2 thin films (i.e. ~100 and 270 nm) as compared to the lateral direction i.e. spacing between adjacent electrodes in few mm. This large space between the Al/CSA-PANI/F-Cl-TiO_2/ITO devices results the higher resistance for current flow to the lateral direction. Thus the dominant current flow in Al/CSA-PANI/F-Cl-TiO_2/ITO system is vertical direction and not in lateral direction. It designate that the vertical charge transport is the governing mechanism for Al/CSA-PANI/F-Cl-TiO_2/ITO structure current conduction whereas the contribution of lateral conduction is negligible with respect to the variation in electrode area or in other words lateral conduction mechanism is utterly ruled out [73,74].

The UV response and saturation behavior of Al/CSA-PANI/F-Cl-TiO_2/ITO, structure is shown in Fig. 5. The heterojunction was subjected to a bias of −1 V to see the maximized effect of UV illumination (wavelength 365 nm and power 35 μW/cm^2) in the reverse bias, and the current was scrutinized by turning the UV light ON and OFF at regular intervals of time (~100 s). Here, the rise time and fall time are defined as the time taken by the current to increase from 10% to 90% and decrease from 90% to 10% of its final value, respectively. From Fig. 5, the rise time and fall time are estimated to be ~0.6 and ~1.6 s, respectively. Therefore, the response of F-Cl-TiO_2/CSA-PANI, n-p heterostructure is acceptable and comparable to other photodetectors which proves its potential candidature for UV photodiode applications. Furthermore, the performance of state-of-the-art UV photodetectors as reported in the literature is summarized in Table 1.

To confirm the observed electrical characteristics are due to the F-Cl-TiO_2/CSA-PANI, n-p heterostructure and not due to formation of composite of F-Cl-TiO_2 and CSA-PANI, it is desired to investigate the cross-sectional structure of the fabricated F-Cl-TiO_2/CSA-PANI, n-p heterostructure. Fig. 6 shows the cross-sectional SEM image of F-Cl-TiO_2/CSA-PANI, n-p heterostructure which clearly indicates demarcation between the deposited CSA-PANI and F-Cl-TiO_2 thin films. From Fig. 6, it is evident that there is no diffusion at the F-Cl-TiO_2/CSA-PANI interface which rules out the possibility of formation of composite at the interface. Moreover, the structural variation in CSA-PANI and F-Cl TiO_2 are recognizable and further confirmed by EDX analysis (graphs are not shown here) with atomic weight% of C 22.30%, N 15.20%, O 54.56%, S 8.80% in CSA-PANI and Ti 1.81%, O 69.58%, F 27.34%, Cl 1.27%, in F-Cl-TiO_2 thin films.

Moreover, to support the observed electrical characteristics of fabricated Al/CSA-PANI/F-Cl-TiO_2/ITO structure, the F-Cl-TiO_2 powder which is used for thin film deposition needs to be investigated. The FESEM micrographs of undoped TiO_2 and F-Cl-TiO_2 powder shown in Fig. 7(a), 7(b), reveals the repeatable structure for both undoped and doped TiO_2. The F-Cl co-doped TiO_2 shows the flake-like structure which indicates the formation of anatase phase on doping with chlorine and fluorine [64,65]. The presence of chlorine reduces the surface area as well as porosity due to the replacement of hydroxyl group (OH^-) on the TiO_2 surface [64]. The atomic weight% of fluorine and chlorine in TiO_2 are confirmed by the EDX analysis. The computed elemental atomic weight% of various species in undoped-TiO_2 and F-Cl co-doped TiO_2 are Ti ~52.7%, O ~47.30% and Ti ~46.35, O ~18.65, F ~1.41, Cl ~33.58, respectively. This significant variation in atomic weight are observed in Oxygen (~29%) from 47.30% to 18.65% and Titanium (~6%) from 52.70% to 46.35% by co-doping F-Cl in TiO_2, is attributed to F^- and Cl^- ions that substitute majority of $O_2{}^-$ ions. F^- being more electronegative replaces the $O_2{}^-$ atoms easily and leads to the enhancement in conductivity, because $O_2{}^-$ will be substituted by F^- which leaves one free electron in the lattice. Moreover, the decrease in Ti weight% may be due to the replacement of Ti-atom by Cl-atom that converts Ti^{4+} to Ti^{3+} thru charge compensation [38]. The replacement of Ti site in TiO_2 exists as Cl^{4+} (s^2p^1) results in instability to the structure, which results in the creation of defects and hence hikes the conductivity of F-Cl-TiO_2 [66].

The effect of doping on the crystallinity of TiO_2 is investigated by the phase analysis of undoped TiO_2 and F-Cl-TiO_2 by XRD diffractograms as shown in Fig. 8. The absence of any rutile/anatase phase of TiO_2 in the undoped TiO_2 samples reveals the amorphous nature of TiO_2 crystallites. Similar, observations were reported earlier by Liu et al. [63]. However, for the case of fluorine and chlorine doped TiO_2 the indexed peaks at 2θ ~31.72°, ~45.38°, ~56.30° are attributed to the reflections from the anatase phase (110), (200) and (006) planes. Here, the increase in crystallinity may be due to the presence of chlorine and fluorine which replaces the TiO_2 surface hydroxyl (OH^-) groups and results in the formation of TiO_2 anatase phase at low temperature (<400 °C) [64,65].

Fig. 9 shows the UV–vis absorption spectra of undoped TiO_2 and F-Cl-TiO_2, where TiO_2 solvent i.e. ethanol is used as the reference for baseline correction. From Fig. 9, it is evident that fluorine and chlo-

Table 1
The progress of UV Photodetectors.

Photodetector Structure	NC-ZnO	*n*-ZnO/*p*-PANI	*n*-TiO_2/p-Si	*n*-Al-B-ZnO/p-Si	*n*-ZnO/p-Si	*n*-ZnO/p-Si	*n*-ZnO/p-GaN	*n*-F-Cl-TiO_2/*p*-CSA-PANI
Operating Voltage	1 V	10 V	10 V	4 V	2 V	5 V	3 V	1 V
Rectification Ratio	–	16	18240	10	145–650	210	4.5–8.6	132
Contrast Ratio	–	46	56704	–	–	120	–	381
Rev. Sat. Current (I_o)	1.29 nA	47 μA	12.2 μA	1.67–2.6 mA	25–87 nA	–	–	6.36 μA
Ideality factor	7.95	–	3.83	1.63–2.40	3.17–4.21	2.3	7–24	1.90
Barrier Height	0.83 eV	0.79 eV	0.81 eV	0.4–0.6 eV	0.68–0.75 eV	0.78 eV	–	0.728 eV
Responsivity	8.5 mA/W	–	1.25 A/W	–	0.34 A/W	0.6 A/W	11 A/W	24.9 A/W
Photoconductive Gain	–	–	4.24	–	–	–	–	84.59
Rise Time	~0.5 s	47 s	–	–	–	0.22 s	0.28 ms	~0.6 s
Fall Time	~1 s	58 s	–	–	–	0.3 s	0.32 ms	~1.6 s
Reference	[9]	[26]	[55]	[59]	[60]	[61]	[62]	This Work

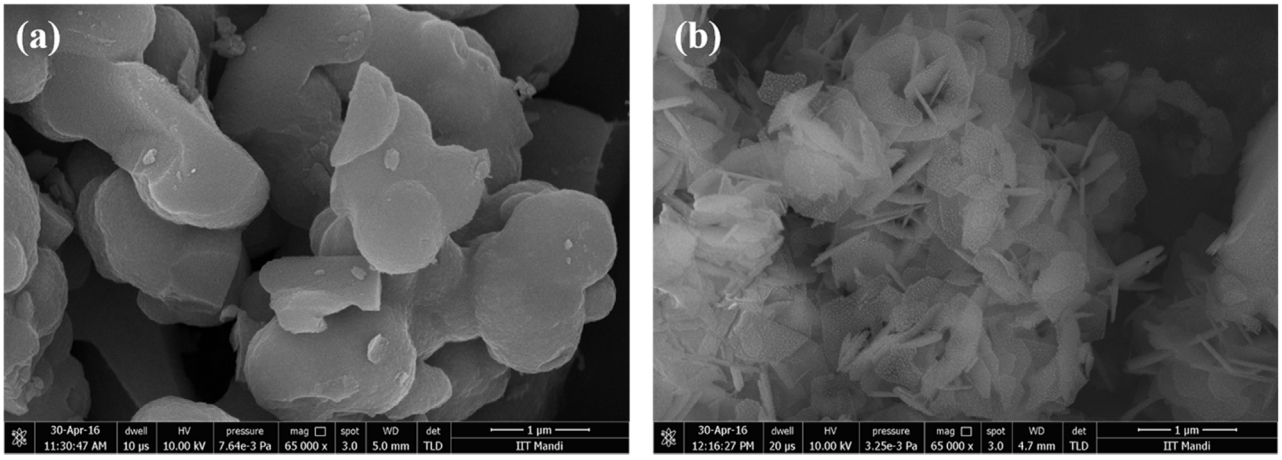

Fig. 7. The Surface micrographs of (a) undoped TiO_2 (b) F-Cl doped TiO_2. The F-Cl doping reduces the surface area as well as porosity in TiO_2 and the flake-like structure confirms the formation of anatase phase in F-Cl-TiO_2.

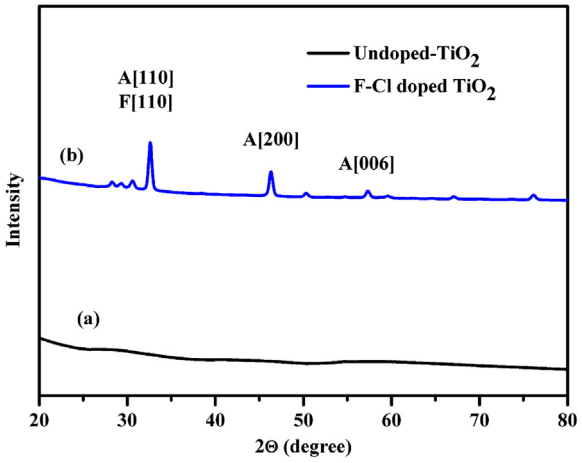

Fig. 8. XRD patterns of (a) Undoped TiO_2, (b) F-Cl doped TiO_2. The F-Cl doping converts the amorphous phase of undoped TiO_2 to the anatase phase in F-Cl-TiO_2.

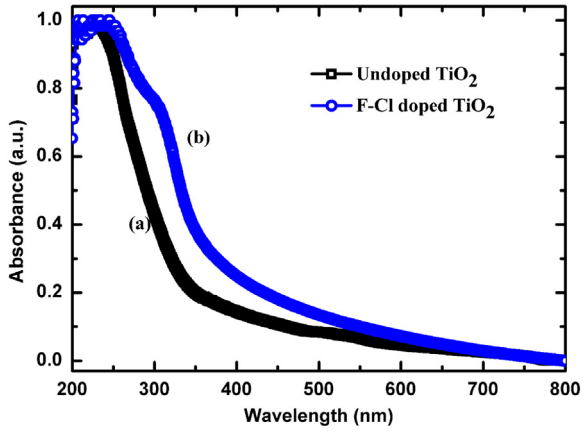

Fig. 9. The normalized UV–vis absorption spectra of (a) undoped TiO_2, (b) F-Cl-TiO_2. Red (Right) Shift is observed in doped TiO_2. (For interpretation of the references to colour in this figure legend, the reader is referred to the web version of this article.)

rine doping in TiO_2 results in the red (right) shift of the absorbance spectrum due to narrowing of the bandgap [67]. The band gap energy (E_g) of TiO_2 is determined by the following fundamental relation:

$$E_g = \frac{hc}{\lambda} \tag{7}$$

where h, c and λ, are the Planck's constant, the velocity of light in vacuum and wavelength of the absorbed radiation, respectively. Using Eq. (7), the band gap of undoped-TiO_2 and F-Cl-TiO_2 is estimated to be ~3.517 and ~3.21 eV, respectively. The reduced bandgap in F-Cl-TiO_2 is attributed to the presence of chlorine and fluorine.

The schematic position of the energy levels and energy band diagram of F-Cl-TiO_2/CSA-PANI, structure, under reverse bias and UV illumination is shown in Fig. 10(a) and 10(b), respectively. Assuming the electron affinity values of CSA-PANI and F-Cl-TiO_2 as 4.7 eV [66,68] and 4.26 eV [67,69]. Likewise, the energy bandgaps of F-Cl-TiO_2 and CSA-PANI are $E_{g,TiO_2} \sim 3.21eV$ and $E_{g,PANI} \sim 2.68$ eV [75], respectively. While, the conduction band and valence band offset is calculated using Anderson's model [56] as $\Delta E_c = \chi_{PANI} -$

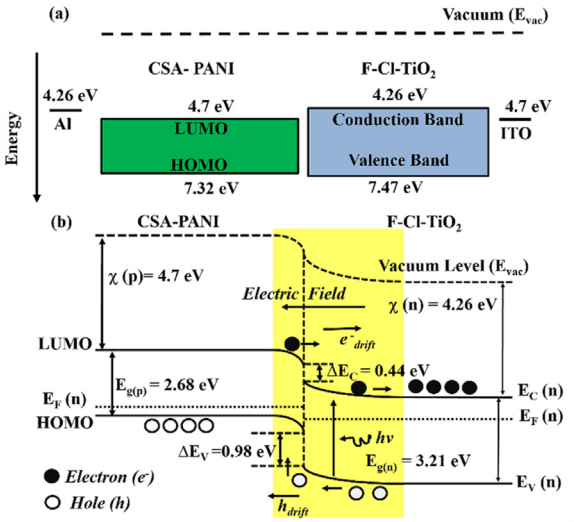

Fig. 10. Schematic energy levels of the F-Cl-TiO_2/CSA-PANI, n-p heterostructure. The energy band diagrams of F-Cl-TiO_2/CSA-PANI, n-p heterostructure under UV illumination under reverse bias condition.

$\chi_{TiO_2} = 0.44eV$ and $\Delta E_c = E_{g,TiO_2} - E_{g,PANI} + \Delta E_c = 0.98eV$, respectively. When UV (365 nm) light ($\lambda \geq E_{g,TiO_2}$) is illuminated, the generation of more number of electron and hole pairs result in the F-Cl-TiO_2 due to the absorption of the photons. Nevertheless, CSA-PANI have the bandgap which is transparent to UV. Additionally, on variation of reverse bias from 0 to −1 V, the depletion region for the generation of electron hole pairs increases (Fig. 10(b) and 2(d)). The generated electron hole pairs in F-Cl-TiO_2 because of the influence of the electric field are dragged away from the depletion region which reduces the area, probability of their recombination and results in the increase of reverse current. While F-Cl-TiO_2/CSA-PANI, n-p heterostructure is in forward bias (+1 V), the depletion region is narrow (Fig. 2(c)), the electric field is small, therefore lower number of electron-hole pairs generation takes place by the absorption of light and recombination is prominent. Therefore, only small amount of the generated electron-hole pairs contribute to the enhancement of forward current on UV illumination.

Finally, a conduction mechanism is proposed to support the effect of doping on the performance of photo diode as shown in Fig. 11. As shown in Fig. 11 that the doping of fluorine and chlorine in TiO_2 induces a new interstitial state i.e. ~F and Cl 2p, sub levels above the O 2p sub levels of valence band which is accountable for reduction in bandgap. Therefore, lower excitation energy is required for electrons to move from valence band to conduction band and results in higher photo conductivity as shown in Fig. 11 [76]. Moreover, the pre-existing defect sites near the valence band of TiO_2 (Fig. 11(a)) act as probable recombination centers for the charge carriers travelling from valence band to conduction band. These interfacial defect sites are filled by the co-doping of the anions (F^- and Cl^-), which allows the electrons to travel from valence band to conduction band with minimum hindrance due to lack of trapping sites and contribute to significant enhancement in photo conductivity. Additionally, the Fluorine and Chlorine anions both replace the oxygen atoms in TiO_2 as revealed from EDX analysis, i.e. $Ti^{4+} \rightarrow Ti^{3+} + e^-$. This formation of extra electron also contributes to the increase in photo current and also the device performance. Although, the contribution of fluorine is dominant as compared to chlorine due to higher electronegativity and smaller atomic size of fluorine. Therefore, the enhanced conductivity of TiO_2 with F and Cl co-doping enhances the performance of the photodiode.

4. Conclusion

In summary, the low cost, simple processing based Al/CSA-PANI/F-Cl-TiO_2/ITO structures are fabricated with acceptable CSA-PANI/F-Cl-TiO_2 interface confirmed by crossectional FESEM analysis. The Al/CSA-PANI/F-Cl-TiO_2/ITO, structures show an excellent rectifying properties with a considerable rectification ratio of ~132 and UV sensitivity of the contrast ratio of ~381 at −1 V. Moreover, it also exhibits an exceptional ideality factor ~1.9, large responsivity ~24.9 A/W, photoconductive gain ~84.59 and reasonable rise/fall time 0.6/1.6 s. The XRD and FESEM analysis reveal that the conversion of the amorphous phase in undoped TiO_2 to the more stable anatase phase in F-Cl-co-doped TiO_2 and also reduces the porosity and surface area. The reduction in band gap of the doped F-Cl-TiO_2 (~3.21 eV) in contrast to undoped (~3.517 eV) is estimated by the UV–vis spectroscopy. It attributes that the F^- and Cl^- ions substitute O^{2-} ions and some of the Ti^{3+} ions. Therefore, the F-Cl-TiO_2/CSA-PANI, n-p heterostructure can be used for next-generation high-performance and low cost photodetection applications.

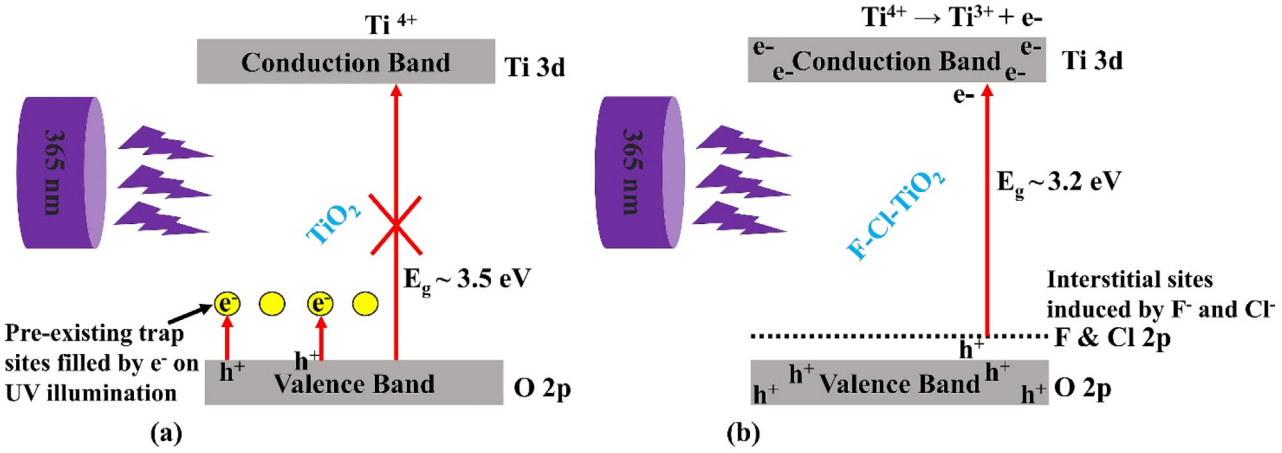

Fig. 11. Schematic diagram for (a) undoped TiO_2 and (b) F-Cl doped TiO_2, showing the proposed mechanism for performance enhancement of photodiode with F and Cl doping in TiO_2.

Acknowledgement

Author S. K. Sharma acknowledges the financial support of seed grant project IIT/SG/SKS/27, Indian Institute of Technology (IIT), Mandi, (H.P), India

References

[1] L. Sang, M. Liao, M. Sumiyo, A comprehensive review of semiconductor ultraviolet photodetectors: from thin film to one-dimensional nanostructure, Sensors 13 (2013) 10482.
[2] B. Guo, G. Wu, H.-Z. Chen, Mang Wang, Solution-processed organic/inorganic hybrid photodetector with selective deep UV sensitivity, Org. Electron. 29 (2016) 13.
[3] T.-H. Chou, Studies of n-SiCN/p-Si diode for low cost and high temperature ultraviolet light sensing applications, Sens. Actuators A 244 (2016) 121.
[4] M.Y. Liao, L.W. Sang, T. Teraji, M. Imura, J. Alvarez, Y. Koide, Comprehensive investigation of single crystal diamond deep-ultraviolet detectors, J. Appl. Phys. 51 (2012) 1 (090115).
[5] W.-C. Lien, D.-S. Tsai, D.-H. Lien, D.G. Senesky, H. He, A.P. Pisano, 4H–SiC metal–semiconductor–metal ultraviolet photodetectors in operation of 450 °C, IEEE Electron. Device Lett. 33 (2012) 1586.
[6] H.-Y. Liu, W.C. Hsu, B.-Y. Chou, Y.-H. Wang, A simple passivation technique for AlGaN/GaN ultraviolet Schottky barrier photodetector, IEEE Photon. Technol. Lett. 26 (2014) 138.
[7] H. Xue, X. Kong, Z. Liu, C. Liu, J. Zhou, W. Chen, S. Ruan, Q. Xu, TiO_2 based metal-semiconductor-metal ultraviolet photodetectors, Appl. Phys. Lett. 90 (2007) (201118-1).
[8] F.H. Alsultany, Z. Hassan, N.M. Ahmed, Low-power UV photodetection characteristics of ZnO tetrapods grown on catalyst-free glass substrate, Sens. Actuators A 250 (2016) 187.
[9] J. Wu, L.Y. Lin, A flexible nanocrystal photovoltaic ultraviolet photodetector on a plant membrane, Adv. Optical Mater. 3 (2015) 1530.
[10] I. Karaduman, M. Demir, D.E. Yıldız, S. Acar, CO_2 gas detection properties of a TIO_2/Al_2O_3 heterostructure under UV light irradiation, Phys. Scr. 90 (2015) 055802.
[11] T. Tsai, S. Chang, T. Hsueh, H. Hsueh, W. Weng, C. Hsu, B. Dai, p-Cu_2O-shell/n-TiO_2-nanowire-core heterostructure photodiodes, Nanoscale Res. Lett. 6 (2011) 1.
[12] M. Vishwas, K.N. Rao, R.P.S. Chakradhar, Influence of annealing temperature on Raman and photoluminescence spectra of electron beam evaporated TiO_2 thin films, Spectrochim. Acta Part A 99 (2012) 33.
[13] A.M. Selman, Z. Hassan, Highly sensitive fast-response UV photodiode fabricated from rutile TiO_2 nanorod array on silicon substrate, Sens. Actuators A: Phys. 221 (2015) 15.
[14] S.N. Mazhir, G.H. Mohamed, A.A. Abdullah, M.D. Radhi, UV photovoltaic detector based on Bi doped TiO_2 fabricated by pulse laser deposition, Int. J. Adv. Res. 3 (2015) 1060.
[15] F. Alema, B. Hertog, O. Ledyaev, D. Volovik, R. Miller, A. Osinsky, S. Bakhshi, W.V. Schoenfeld, High responsivity solar blind photodetector based on high Mg content MgZnO film grown via pulsed metal organic chemical vapor deposition, Sens. Actuators A 249 (2016) 263.
[16] A.M. Selman, Z. Hassan, M. Husham, N.M. Ahmed, A high sensitivity, fast-response, rapid-recovery p-n heterojunction photodiode based on rutile TiO_2 nanorod array on p-Si (111), Appl. Surf. Sci. 305 (2014) 445.
[17] P.S. Shinde, P.S. Patil, P.N. Bhosale, A. Brüger, G. Nauer, M. Neumann-Spallart, C.H. Bhosale, UVA and solar light assisted photoelectrocatalytic degradation of AO7 dye in water using spray deposited TiO_2 thin films, Appl. Catal. B: Environ. 89 (2009) 288.
[18] Y. Xie, H. Huang, W. Yang, Z. Wu, Low dark current metal semiconductor-metal ultraviolet photodetectors based on sol-gel derived TiO_2 films, J. Appl. Phys. 109 (2011) 023114.
[19] H. Zhang, S. Ruan, H. Li, M. Zhang, K. Lv, C. Feng, W. Chen, Schottky diode ultraviolet detector based on TiO_2 nanowire array, IEEE Electron. Device Lett. 33 (2012) 83.
[20] R. Mechiakh, N. Ben Sedrine, J. Ben Naceur, R. Chtourou, Elaboration and characterization of nanocrystalline TiO_2 thin films prepared by sol–gel dip-coating, Surf. Coat. Technol. 206 (2011) 243.
[21] A.B. Yadav, A. Pandey, D. Somvanshi, S. Jit, Sol-gel-based highly sensitive Pd/n-ZnO thin film/n-Si schottky ultraviolet photodiodes, IEEE Trans. Electron Devices 62 (2015) 1879.
[22] P. Panagiotopoulou, D.I. Kondarides, X.E. Verykios, Mechanistic study of the selective methanation of CO over Ru/TiO_2 catalyst: identification of active surface species and reaction pathways, J. Phys. Chem. C 115 (2011) 1220.
[23] H.B. Liu, Y.M. Wu, J.L. Zhang, A new approach toward carbon-modified vanadium-doped titanium dioxide photocatalysts, ACS Appl. Mater. Interfaces 3 (2011) 1757.
[24] Y.-B. Tang, L.-C. Yin, Y. Yang, X.-H. Bo, Y.-L. Cao, H.-E. Wang, W.-J. Zhang, I. Bello, S.-T. Lee, H.-M. Cheng, C.-S. Lee, Tunable band gaps and p-type transport properties of boron-doped graphenes by controllable ion doping using reactive microwave plasma, ACS Nano 6 (2012) 1970.
[25] S.K. Parayil, H.S. Kibombo, C.M. Wu, R. Peng, J. Baltrusaitis, R.T. Koodali, Enhanced photocatalytic water splitting activity of carbon-modified TiO_2 composite materials synthesized by a green synthetic approach, Int. J. Hydrogen Energy 37 (2012) 8257.
[26] S. Mridha, D. Basak, ZnO/polyaniline based inorganic/organic hybrid structure: electrical and photoconductivity properties, Appl. Phys. Lett. 92 (2008) 142111.
[27] S. Virji, J. Huang, R.B. Kaner, B.H. Weiller, Polyaniline nanofiber gas sensors: examination of response mechanisms, Nano Lett. 4 (2004) 491.
[28] A.G. MacDiarmid, A.J. Epstein, Secondary doping in polyaniline, Synth. Met. 69 (1995) 85.
[29] O.A. Razzaq, S.E. Bourdo, M. Woo, V. Saini, B.C. Berry, A. Ghosh, A.S. Biris, Comparative aging study of organic solar cells utilizing polyaniline and PEDOT:PSS as hole transport layers, Appl. Mater. Interfaces 7 (2015) 27667.
[30] S. Yuan, Y. Chen, L.Y. Shi, J.H. Fang, J.P. Zhang, J.L. Zhang, H. Yamashita, Synthesis and characterization of Ce-doped mesoporous anatase with long-range ordered mesostructure, Mater. Lett. 61 (2007) 4283.
[31] J.F. Zhu, Z.G. Deng, F. Chen, J.L. Zhang, H.J. Chen, M. Anpo, J.Z. Huang, Z.L. Zhang, Hydrothermal doping method for preparation of Cr^{3+}-TiO_2photocatalysts with concentration gradient distribution of Cr^{3+}, Appl. Catal. B 62 (2006) 329.
[32] Y. Yang, C.X. Tian, Effects of calcining temperature on photocatalytic activity of Fe-doped sulfated titania, Photochem. Photobiol. 88 (2012) 816.
[33] H.T. Gao, W.C. Liu, B. Lu, F.F. Liu, Photocatalytic activity of La, Y Co-doped TiO_2 nanoparticles synthesized by ultrasonic assisted sol-gel method, J. Nanosci. Nanotechnol. 12 (2012) 3959.
[34] H. Seo, L.R. Baker, A. Hervier, J. Kim, J.L. Whitten, G.A. Somorjai, Generation of highly n-type titanium oxide using plasma fluorine insertion, Nano Lett. 11 (2011) 751.
[35] J.L. Zhang, M. Matsuoka, H. Yamashita, M. Anpo, XAFS studies on the local structure of Ti-HMS mesoporous molecular sieves and their photocatalytic properties, J. Synchrotron Radiat. 8 (2001) 637.
[36] K. Yang, Y. Dai, B.J. Huang, Understanding photocatalytic activity of S- and P-doped TiO_2 under visible light from first-principles, Phys. Chem. C 111 (2007) 18985.
[37] Y. Niu, M. Xing, B. Tian, J. Zhang, Improving the visible light photocatalytic activity of nano-sized titanium dioxide via the synergistic effects between sulfur doping and sulfation, Appl. Catal. B 115–116 (2012) 253.
[38] J. Schneider, M. Matsuoka, M. Takeuchi, J. Zhang, Y. Horiuchi, M. Anpo, D.W. Bahnemann, Understanding TiO_2 photocatalysis: mechanisms and materials, Chem. Rev. 114 (2014) 9919.
[39] S. Tojo, T. Tachikawa, M. Fujitsuka, T. Majima, Iodine-doped TiO_2 photocatalysts: correlation between band structure and mechanism, J. Phys. Chem. C 112 (2008) 14948.
[40] X.-K. Wanga, C. Wanga, W.-Q. Jianga, W.-L. Guoc, J.-G. Wang, Sonochemical synthesis and characterization of Cl-doped TiO2 and its application in the photodegradation of phthalate ester under visible light irradiation, Chem. Eng. J. 189–190 (2012) 288.
[41] H. Luo, T. Takata, Y. Lee, J. Zhao, K. Domen, Y. Yan, Photocatalytic activity enhancing for titanium dioxide by Co-doping with bromine and chlorine, Chem. Mater. 16 (2004) 846.
[42] S. Chakrabartty, A. Mondal, M.B. Sarkar, B. Choudhuri, A.K. Saha, A. Bhattacharyya, TiO_2 nanoparticles arrays ultraviolet-A detector with Au schottky contact, IEEE Photon. Technol. Lett. 26 (2014) 1065.
[43] P. Chinnamuthu, J.C. Dhar, A. Mondal, A. Bhattacharyya, N.K. Singh, Ultraviolet detection using TiO_2 nanowire array with Ag Schottky contact, J. Phys. D. Appl. Phys. 45 (2012) 135102.
[44] N.M. Abd-Alghafour, N.M. Ahmed, Z. Hassan, Fabrication and characterization of V_2O_5 nanorods based metal–semiconductor–metal photodetector, Sens. Actuators A 250 (2016) 250.
[45] A. Hazra, P.P. Chattopadhyay, P. Bhattacharyya, Hybrid fabrication of highly rectifying p-n homojunction based on nanostructured TiO_2, IEEE Electron Device Lett. 36 (2015) 505.
[46] M. Zhang, H. Zhang, K. Lv, W. Chen, J. Zhou, L. Shen, S. Ruan, Ultraviolet photodetector with high internal gain enhanced by $TiO_2/SrTiO_3$ heterojunction, Opt. Express 20 (2012) 5936.
[47] Z. Liu, J. Zhou, H. Xue, L. Shen, H. Zang, W. Chen, Polyaniline/TiO_2 solar cells, Synth. Met. 156 (2006) 721.
[48] S. Ameen, M. Song, D.-G. Kim, Y.-B. Im, H.-K. Seo, Y.S. Kim, H.-S. Shin, Iodine doped polyaniline thin film for heterostructure devices via PECVD technique: morphological, structural, and electrical properties, Macromol. Res. 20 (2012) 30.
[49] S. Ameen, M.S. Akhtar, Y.S. Kim, O.B. Yang, H.-S. Shin, Diode behavior of electrophoretically deposited polyaniline on TiO_2Nanoparticulate thin film electrode, J. Nanosci. Nanotechnol. 11 (2011) 1559.
[50] M.V. Dozzi, C.D. Andrea, B. Ohtani, G. Valentini, Elena Selli, Fluorine-doped TiO_2 materials: photocatalytic activity vs time-resolved photoluminescence, J. Phys. Chem. C 117 (2013) 25586.
[51] H. Xu, Z. Zheng, L. Zhang, H. Zhang, F. Deng, Hierarchical chlorine-doped rutile TiO_2 spherical clusters of nanorods: large-scale synthesis and high photocatalytic activity, J. Solid State Chem. 181 (2008) 2516.
[52] U.K. Mishra, J. Singh, Semiconductor Device Physics and Design, Springer, The Netherlands, 2008.
[53] H. Zhang, S. Ruan, H. Li, M. Zhang, K. Lv, C. Feng, W. Chen, Schottky diode ultraviolet detector based on TiO_2 nanowire array, IEEE Electron Device Lett. 33 (2012) 83.
[54] S.M. Sze, Physics of Semiconductor Devices, Wiley, New York, USA, 1981.
[55] G. Rawat, D. Somvanshi, H. Kumar, Y. Kumar, C. Kumar, S. Jit, Ultraviolet detection properties of p-Si/n-TiO_2 heterojunction photodiodes grown by

electron-beam evaporation and sol–gel methods: a comparative study, IEEE Trans. Nanotechnol. 15 (2016) 193.
[56] H. Huang, W. Yang, Y. Xie, X. Chen, Z. Wu, Metal-Semiconductor-metal ultraviolet photodetectors based on TiO_2 films deposited by radio-Frequency magnetron sputtering, IEEE Electron Device Lett. 31 (2010) 588.
[57] P. Hazra, S.K. Singh, S. Jit, Ultraviolet photodetection properties of ZnO/Si heterojunction diodes fabricated by ALD technique without using a buffer layer, J. Semicond. Technol. Sci. 14 (2014) 117.
[58] C. Soci, A. Zhang, B. Xiang, S.A. Dayeh, D.P.R. Aplin, J. Park, X.Y. Bao, Y.H. Lo, D. Wang, ZnO nanowire UV photodetectors with high internal gain, Nano Lett. 7 (2007) 1003.
[59] V. Kumar, N. Singh, A. Kapoor, O.M. Ntwaeaborwa, H.C. Swart, Fabrication and characterization of n-type aluminum-boron co-doped ZnO on p-type silicon (n-AZB/p-Si) heterojunction diodes, Mater. Res. Bull. 48 (2013) 4596.
[60] S.K. Singh, P. Hazra, S. Tripathi, P. Chakrabarti, Performance analysis of RF-sputtered ZnO/Si heterojunction UV photodetectors with high photo-responsivity, Superlattices Microstruct. 91 (2016) 62.
[61] N.H. Al-Hardan, M.A.A. Hamid, N.M. Ahmed, R. Shamsudin, N.K. Othman, Ag/ZnO/p-Si/Ag heterojunction and their optoelectronic characteristics under different UV wavelength illumination, Sens. Actuators A 242 (2016) 50.
[62] L.S. Vikas, K.A. Vanaja, P.P. Subha, M.K. Jayaraj, Fast UV sensing properties of n-ZnO nanorods/p-GaN heterojunction, Sens. Actuators A 242 (2016) 116.
[63] S. Liu, L. Han, Y. Duan, S. Asahina, O. Terasaki, Y. Cao, B. Liu, L. Ma, J. Zhang, S. Che, Synthesis of chiral TiO_2 nanofibre with electron transition-based optical activity, Nat. Commun. 3 (2012) 1215.
[64] A.G. Shastri, A.K. Datye, J. Schwank, Influence of chlorine on the surface area and morphology of TiO_2, Appl. Catal. 14 (1985) 119.
[65] J. Yua, J.C. Yu, M.K.-P. Leung, W. Ho, B. Chenga, X. Zhao, J. Zhao, Effects of acidic and basic hydrolysis catalysts on the photocatalytic activity and microstructures of bimodal mesoporous titania, J. Catal. 217 (2003) 69.
[66] K. Yang, Y. Dai, B. Huang, M.-H. Whangbo, Density functional characterization of the band edges, the band gap states and the preferred doping sites of halogen doped TiO_2, Chem. Mater. 20 (2008) 6528.
[67] J.M. Coronado, F. Fresno, M.D.H. -Alonso, R. Portela, Design of advanced photocatalytic materials for energy and environmental applications, Springer—Green Energy Technol. (2013).
[68] M. Liess, D. Chinn, D. Petelenz, J. Janata, Properties of insulated gate field-effect transistors with a polyaniline gate electrode, Thin Solid Films 286 (1996) 252.
[69] I. Chung, B. Lee, J. He, R.P.H. Chang, M.G. Kanatzidis, All-solid-state dye-sensitized solar cells with high efficiency, Nature 485 (2012) 486.
[70] C. Dhand, M. Das, M. Datta, B.D. Malhotra, Recent advances in polyaniline based biosensors, Biosens. Bioelectron. 26 (2011) 2811.
[71] R.H. Austin, S.-F. Lim, The Sackler Colloquium on promises and perils in nanotechnology for medicine, PNAS 105 (2008) 17217.
[72] A. Kobayashi, H. Ishikawa, K. Amano, M. Satoh, E. Hasegawa, Electrical conductivity of annealed polyaniline, J. Appl. Phys. 74 (1993) 296.
[73] U. Shafique, K.S. Karim, Lateral organic semiconductor photodetector: effect of electrode spacing, IEEE J. Select. Top. Quant. Electron. 23 (2017) 3800807.
[74] F. Guo, B. Yang, Y. Yuan, Z. Xiao, Q. Dong, Y. Bi, J. Huang, A nanocomposite ultraviolet photodetector based on interfacial trap-controlled charge injection, Nat. Nanotechnol. 7 (2012) 798.
[75] Q.A. Acton, Advances in nanotechnology research and application, technology & engineering, Scholarly Ed. (2012).
[76] S.A. Ansari, M.M. Khan, M.O. Ansari, M.H. Cho, Nitrogen-doped titanium dioxide (N-doped TiO_2) for visible light photocatalysis, New J. Chem. 40 (2016) 3000.

Biographies

Shivani Sharma was born in Himachal Pradesh, India. She received her B. Tech (electronics and communication engineering) from Eternal University, Himachal Pradesh, India and M. Tech (VLSI Technology) from Graphic Era University, Dehradun, India in 2012 and 2014, respectively. She is currently working towards the Ph.D degree with school of computing and electrical engineering at Indian Institute of Technology (IIT) – Mandi, Himachal Pradesh, India. Her research interests include organic electronics and photodetectors.

Robin Khosla was born in Punjab, India, in 1989. He received the B. Tech (electronics and communication engineering) and M. Tech (VLSI Design) degree from Punjab Technical University, Punjab, India in 2011 and 2013, respectively. He is currently working towards the Ph.D degree with school of computing and electrical engineering at Indian Institute of Technology (IIT) – Mandi, Himachal Pradesh, India. His research interests include fabrication, characterization and reliability of high-κ dielectrics for CMOS and non-volatile memory applications.

Dinesh Deva was born in Kanpur, India in 1963. He received the M.Sc. degree in Physics from Indian Institute of Technology (IIT) – Roorkee, Uttrakhand, India in 1985. He received the M.Tech. degree in Materials Science from Indian Institute of Technology (IIT) – Kanpur, Uttar Pradesh, India in 1987. He received Ph.D. from CSJM University and Indian Institute of Technology (IIT) – Kanpur, Uttar Pradesh, India in 2008. From 2011 to 2014, he worked as Consultant at the DST Unit on Nanosciences, Department of CHE, Indian Institute of Technology (IIT) – Kanpur, Uttar Pradesh, India. From 2014 to 2016, he worked as consultant for industrial sponsored project at IIT Kanpur. He is currently working as Consultant for thedevelopment of Centre for Design and Fabrication of Electronic Devices (C4DFED) at Indian Institute of Technology (IIT) – Mandi, Himachal Pradesh, India.

Hitesh Shrimali was born in Ahmedabad, Gujarat India. He Received bachelor of Engineering (BE) and master of technology (M.Tech) from Nirma institute of technology and IIT Kharagpur, respectively in instrumentation Engineering. After that he received his PhD in VLSI design from IIT Delhi. After completing his education, he has worked with ST microelectronics, INDIA for two years (Aug 2011–June 2013) in the technology R&D department of analog to digital converter team of analog and mixed signal group. He was a post doctorate researcher with UniversitàdegliStudi di Milano from June 2013–dec 2014. Since dec14 he is serving IIT MANDI as an assistant professor. His area of expertise includes Design and testing of radiation hard circuits [CMOS silicon detectors], Analog and mixed signal VLSI design [ADCs], Modeling of radiation effects on analog and mixed signal circuits and On-chip Instrumentation.

Satinder Kumar Sharma was born in Himachal Pradesh, India in 1978. He received the M.Sc. degree in Physics (Electronics Science) from Himachal Pradesh University, Shimla (H.P.), India in 2002 and Ph.D. from Department of Electronics Science, on "Silicon based gate dielectric materials for VLSI/ULSI Technology" Kurukshetra University, Kurukshetra-(Haryana), India, in 2007. From 2007 to 2010 he worked as a Post-Doctoral Fellow in DST-Unit on Nanosciences and Nanotechnology, Department of CHE, at Indian Institute of Technology (IIT) – Kanpur, India. He worked as a faculty in Electronics and Microelectronics Division, Indian Institute of Information Technology (IIIT)-Allahabad, India from 2010 to 2012. He is currently, an Associate Professor, School of Computing and Electrical Engineering (SCEE), Indian Institute of Technology (IIT) – Mandi, (Himachal Pradesh), India. His current research interests include Microelectronics circuits and system, CMOS device, fabrication & characterization, Nano/Micro fabrication & design, polymer nano composite, Sensors, Photovoltaic & self-assembly.